Design of optimal rule-based controller for plug-in series hybrid electric vehicle

Hussein Basma, Houssam Halaby, Anis Baz Radwan, Charbel Mansour

Design of optimal rule-based controller for plug-in series hybrid electric vehicle

Conference Paper · June 2019

CITATIONS
0

READS
2

4 authors, including:

Hussein Basma
PSL Research University
2 PUBLICATIONS **0** CITATIONS
SEE PROFILE

Charbel Mansour
Lebanese American University
22 PUBLICATIONS **130** CITATIONS
SEE PROFILE

Design of optimal rule-based controller for plug-in series hybrid electric vehicle

Hussein Basma [a], Houssam Halaby [b], Anis Baz Radwan [c] and Charbel J. Mansour [d]

*[a] PSL Research University - Mines ParisTech, Paris, CES- Centre d'efficacité énergétique des systèmes France, hussein.basma@mines-paristech.fr (**CA**)*
[b] Institut Français du Pétrole (IFP), Center for IC Engines and Hydrocarbons Utilizations, Rueil Malmaison, France, houssam.halaby@lau.edu
[c] University of South Carolina, Mechanical Engineering Department, South Carolina, United States of America, anisb@email.sc.edu
[d] Lebanese American University, Industrial and Mechanical Engineering Department, New York, United States of America, charbel.mansour@lau.edu.lb

Abstract:
Energy consumption of Hybrid Electric Vehicles (HEV) strongly depends on the adopted energy management strategy (EMS). Rule-Based (RB) controllers are the most commonly used for their ability of integration in real-time applications. Unlike global optimization routines, RB controllers do not ensure optimal energy savings. This study presents a methodology to design a close-to-optimal RB controller derived from global optimization strategies. First, dynamic programming (DP) optimization is used to derive the optimal behaviour of the powertrain components on the Worldwide Harmonized Light Vehicles Test Cycle (WLTC), and then, the resulting performance of the powertrain components is used to design an optimized RB energy management strategy. Furthermore, the strategy is developed to cope with the variations in trip length and traffic conditions. The plug-in series hybrid electric vehicle is modelled using the energetic macroscopic representation (EMR). Results show that the proposed optimal RB controller is only consuming 1-2% more fuel compared to DP controllers and is resulting in a 13 – 16% less fuel consumption compared to basic RB controllers.

Keywords:
Plug in series hybrid electric vehicle, Energy management strategies, Adaptive controller, Rule-based control, Energetic macroscopic representation.

1. Introduction

Environmental concerns have been the leading drive behind the hybrid technologies emerging in the automotive industry. A considerable amount of effort is spent on designing fuel efficient vehicles that can meet the consumer's demands of functionality and comfort and maintain a low level of emissions. Electric vehicles (EV), hybrid electric vehicles (HEV) and plug-in hybrid vehicles (PHEV) have emerged as viable solutions to these concerns, with focus being directed on HEVs and PHEVs as the transition phase between conventional vehicles and fully electric vehicles.

The energy consumption of these vehicles is highly dependent on their energy management strategy (EMS). The EMS in HEVs decides on the instantaneous power request from the different energy sources. Different control strategies have been deployed in HEVs. HEVs control strategies can be categorized into two main groups, optimization-based control and rule-based control. Optimization based controllers aim to minimize a cost function over a predefined trip. The cost function is defined in general as the vehicle energy consumption or emissions. In contrast, rule-based controllers are fundamental controllers that depend on the vehicle mode of operation where rules are established based on heuristics, engineering intuition or even mathematical models [1,2].

Optimization based EMS is based on defining a cost function which sums all the objective functions to be minimized [3]. The cost function may include fuel consumption, emissions, torque, battery aging, etc. … depending on the application [1]. Optimization based EMS are split into two main sub-categories, global optimization strategies and local optimization strategies. Global optimization strategies can introduce a global optimum solution for a defined cost function [4]. These strategies require a prior knowledge of the entire trip including the route, driver's response, driving behaviour and the battery SOC [1]. This makes global optimization strategies unimplementable in real time, in addition to their computational complexity [2]. Many studies introduce global optimization strategies in HEV control such as Linear Programming in [5] , Dynamic Programming (DP) in [6,7] and genetic algorithm in [8,9]. On the other hand, local optimization-based strategies split the global optimization problem into a series of local optimization problems reducing the computational burden [3]. Local optimization-based strategies such as PMP (Pontryagin's Minimum Principle) and ECMS (Equivalent Consumption Minimization Strategy) are widely deployed in HEVs. Many studies [10,11] used PMP as an optimal or close to optimal EMS. In addition, Many studies [12,13] have used ECMS as an EMS in HEV. Optimization-based EMS cannot be implemented in real time, except for ECMS, which still needs prior knowledge of the trip to attain its close-to-optimal control.

The second major type of EMS in HEV is RB controllers. They consist of a set of rules that are initially predefined without any prior knowledge of the trip [14]. These rules are further calibrated using vehicle simulations. RB controllers can be easily implemented in real time application [1], however, they cannot guarantee optimal behaviour of the powertrain components [3]. There are two main types of RB controllers, deterministic RB and fuzzy RB controllers. Deterministic RB controllers are subdivided into two types: the thermostat (ON-OFF) control strategy used in [15] and the power follower strategy where the engine is the sole power supply and the electric machine supplies additional power whenever needed by the vehicle [1–4,14]. On the other hand, Fuzzy RB controllers are an extension of the deterministic RB control strategy. However, the rules here are not mathematically precise [4]. The core of fuzzy RB control is that it is based on approximation rather than precision, making it adaptive to some extent [3]. The simplest type of fuzzy RB controller is the conventional/traditional fuzzy control. It is developed to force the engine to operate on its optimal efficiency line using load balance by means of the electric machine [3]. In addition, adaptive fuzzy RB control is deployed in HEV as well. It can ensure close-to-optimal control if its inputs are well tuned. The last type of fuzzy control is predictive fuzzy RB control which is based on real-time control and data collected using the global positioning system (GPS).

Building on the findings, the review of these studies underlines the following two gaps:

- There is no comprehensive methodology to design, in few steps, an RB EMS for HEV with close to optimal powertrain components behaviour.

- Current RB EMS for HEV cannot capture variations in trip distance lengths and traffic intensities without implementing complicated driving pattern recognitions.

Therefore, based on the above synthesis of the insights and gaps in the literature, this study proposes a comprehensive methodology to help powertrain-modelling practitioners to design in few steps an EMS for HEV that provides close to optimal consumption results.

2. Vehicle modelling setup

2.1. Powertrain architecture: series plug-in hybrid electric vehicle

A plug-in series HEV is considered in this study. Vehicle parameters are obtained from the second-generation series-parallel TOYOTA PRIUS and modified accordingly to fit the purpose of this study. The powertrain includes a 50-kW electric machine to drive the vehicle and recover braking energy, and a 1.5 L, 57 kW Atkinson engine mechanically connected to a 50-kW electric generator (EG) to act as the auxiliary power unit (APU). The previous 1.3 kWh TOYOTA Prius Nickel-Metal (NiMH) battery is upgraded to 5.1 kWh and operates in the range of 80% to 30% state of charge (SOC). The vehicle parameters are summarized in Table 1. The powertrain is shown in Figure 1.

2.2. Modelling technique: energetic macroscopic representation

Energetic Macroscopic Representation (EMR) is a graphical tool that describes electromechanical systems based on their components interactions [16]. This technique proved very useful in simulating the power flows in HEV powertrains. Powertrain elements are represented graphically by blocks and are divided into four types: Source/Sink elements, Conversion elements, Accumulation elements, and Coupling elements. Each element has input and output vectors representing its action/reaction relations with the adjacent elements. The product of each pair of vectors between adjacent elements represents the instantaneous power exchange between them. This is defined as the interaction principle [17]. This way of representation allows the deduction of a control strategy by applying the inversion principle. This method is called inversion-based control (IBC) and dictates the inversion of each element. The control structure of a system is considered an inversion model of the system because the control must define the appropriate inputs to achieve a desired output. In this method, relationships without time-dependence are directly inverted. However, following the integral causality principle, a direct inversion of time-dependent relationships is not possible. An indirect inversion is thus considered using proportional – integral (PI) controller [17].

Table 1: Vehicle Parameters

Parameter	Description	Value
m_{veh}	Vehicle mass	1420 kg
f_0	Friction coefficient 0	195
f_1	Friction coefficient 1	0.3389
f_2	Friction coefficient 2	0.0296
r_{wheel}	Wheel radius	0.301 m
r_{diff}	Differential ratio	4.113
r_{eg}	Engine/EG ratio	1
η_{diff}	Differential efficiency	0.98
η_{gb}	Gear efficiency	0.95
Q_{LHV}	Lower heating value of gasoline	42.3 MJ/kg
P_{aux}	Auxiliaries power	300 W
Q_b	Battery capacity	5.1 kWh

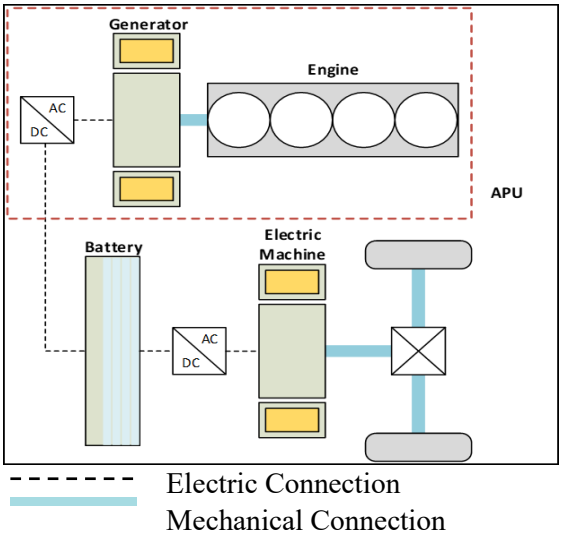

Figure 1: Series powertrain architecture

2.3. EMR and IBC of the studied powertrain

The EMR model of the studied series PHEV is demonstrated in Figure 2. The fuel tank and battery form the energy storage unit of the vehicle. The flow of electric energy from the EG, battery and EM are coupled in an inverter. The EM, differential and wheels form the traction unit. The transmission includes only the differential.

The IBC is also shown in Figure 2. The tuning path, which is the set of variables that form the control loop, has two tuning inputs: the reference braking force F_{brake_ref}, and the reference torque of the EM. These tuning inputs will control the vehicle speed. Thus, the elements to be inverted are the chassis, mechanical coupling, wheels, and driveline. The APU and energy storage unit are not included in the tuning path, since they are controlled and tuned by the EMS, which is detailed further in section 3.

2.3.1. Multi-physical conversion elements

The multi-physical conversion elements convert energy from one form to another.

The ICE, EG, and EM are all multi-physical conversion elements.

ICE model: The engine is utilized to convert the chemical energy of the fuel into mechanical work that drives the EG. The fuel consumption is calculated as follows:

$$\dot{m}_{fuel}(t) = \frac{\omega_{ICE}(t) \times T_{ICE}(t)}{Q_{LHV} \times \eta_{ICE}(t)} \tag{1}$$

where T_{ICE} is the engine torque, ω_{ICE} is the engine speed, and η_{ICE} is the engine efficiency computed from the engine performance map.

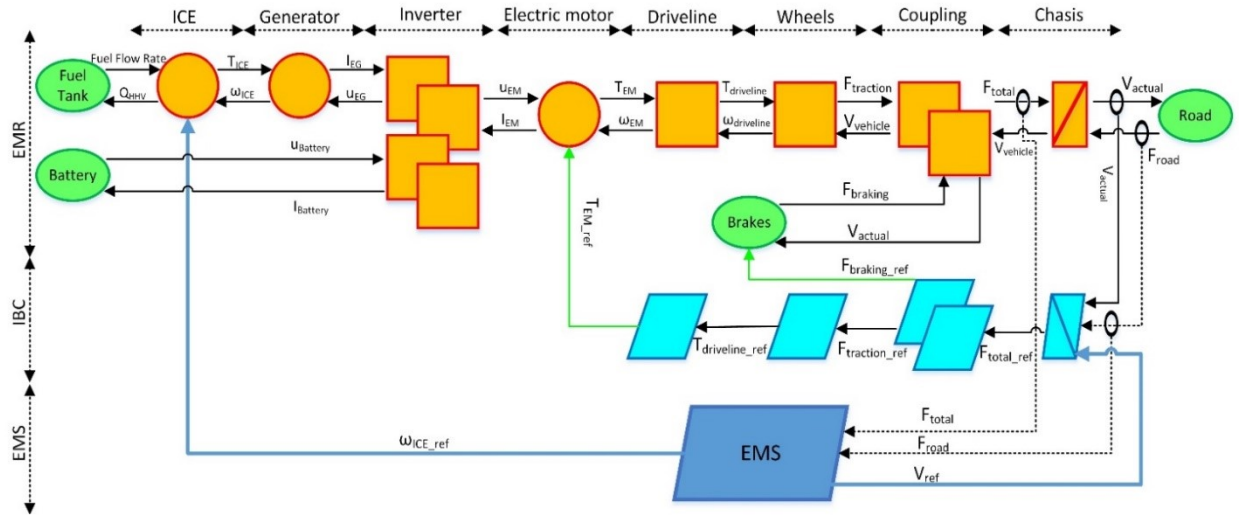

Figure 2: Energetic Macroscopic Representation and Inversion-Based Control of the investigated series hybrid powertrain

Electric Generator model: The 50-kW EG is connected directly to the ICE and is used to charge the battery. Generator torque (T_{EG}) speed (ω_{EG}) electric power (P_{EG}) and current (I_{EG}) are calculated as follows:

$$T_{EG}(t) = \frac{1}{K_{EG}} T_{ICE}(t) \tag{2}$$

$$\omega_{EG}(t) = K_{EG}\omega_{ICE}(t) \tag{3}$$

$$P_{EG}(t) = \omega_{EG}(t) T_{EG}(t) \eta_{EG}(t) \quad (4)$$

$$I_{EG}(t) = \frac{P_{EG}(t)}{u_{EG}(t)} \quad (5)$$

where K_{EG} is the gear ratio between the engine and the EG, η_{EG} is the EG efficiency, and u_{EG} is the EG voltage.

Electric machine model: In the Series architecture, the wheels are mechanically coupled to the electric machine. Thus, the EM needs to meet the total requested load power P_l. It operates in two modes, traction mode and brake energy recovery (BER) mode, depending on whether P_l is positive or negative. During braking, the EM recovers kinetic energy and consequently charges the battery. The braking torque recovery is limited by the maximum torque of the EM and the battery SOC. The torque T_{EM} is determined from the IBC as a tuning parameter, T_{EM_ref} . The current, I_{EM}, is calculated depending on the operating mode:

$$I_{EM}(t) = \frac{T_{EM}(t)\omega_{EM}(t)}{u_{EM}(t)\eta_{EM}^{k}(t)} \quad (6)$$

where u_{EM} is the EM voltage, η_{EM}^{k} is the efficiency of the EM and k take the values of 1 or -1, depending on the operating mode of the EM.

2.3.2. Mono-physical conversion elements:

The mono-physical conversion elements transmit energy without changing its form such as the driveline and the wheels.

Driveline Model: Since the series architecture does not include a gearbox, the differential is modeled as the only transmission element in the powertrain. The driveline torque ($T_{driveline}$) and speed ($\omega_{driveline}$) are calculated as follows:

$$T_{driveline}(t) = \frac{1}{K_D} T_{EM}(t) \eta_{trans} \quad (7)$$

$$\omega_{driveline}(t) = K_D \omega_{EM}(t) \quad (8)$$

where K_D is the final drive ratio and η_{trans} is the driveline efficiency.

Wheels model: The wheels model is simplified and considered as a single wheel receiving all the torque from the driveline. The traction force ($F_{traction}$) and the resulting vehicle velocity (V_{veh}) are calculated as follows:

$$F_{traction}(t) = \frac{T_{driveline}(t)}{r_{wheel}} \quad (9)$$

$$V_{veh}(t) = \frac{\omega_{driveline}(t)}{r_{wheel}} \quad (10)$$

where r_{wheel} is the wheel radius.

2.3.3. Coupling elements

The coupling elements couples 2 or more energy inputs of similar form such as the electric and mechanical coupling.

Electric Coupling: This element receives currents from the EG and the EM, and outputs the resulting battery current, I_{bat}. I_{bat} is negative during discharge mode and positive during charging

mode. The battery, EG, and EM are electrically connected in parallel and hence obey the following equations:

$$u_{bat}(t) = u_{EG}(t) = u_{EM}(t) \tag{11}$$

$$I_{bat}(t) = I_{EG}(t) + I_{EM}(t) + I_{aux}(t) \tag{12}$$

where I_{EG} is the EG current and I_{aux} is the current demanded by the auxiliaries of the vehicle. I_{EG} is positive since the EG only charges the battery, and I_{aux} is obviously negative.

Mechanical Coupling: The mechanical coupling receives the forces $F_{traction}$ and $F_{braking}$ acting on the wheels and outputs the total force, F_{total}, driving the vehicle chassis as follows:

$$F_{total}(t) = F_{traction}(t) + F_{braking}(t) \tag{13}$$

Where naturally $F_{traction}(t)$ is a positive quantity and $F_{braking}(t)$ is a negative one. Note that the vehicle controller avoids actuating these two forces simultaneously.

2.3.4. Accumulation elements

The accumulation elements are time dependent elements that accumulate energy and cannot be inverted directly. In this model, only the vehicle chassis is treated as an accumulation element. The inertias of the different driveline components are neglected.

Chassis: The energy is accumulated in the chassis in the form of kinetic energy where the velocity is computed as follows:

$$V_{veh}(t) = \int_{n}^{n+1} \frac{\left(F_{total}(t) - F_{road}(t)\right)}{M} dt \tag{14}$$

with M is the mass of the vehicle and F_{road} is the sum of the resistive forces acting on the vehicle, calculated as follows:

$$F_{road}(t) = f_0 + f_1(V_{veh}(t)) + f_2(V_{veh}(t))^2 \tag{15}$$

Where F_0 represents rolling resistance, F_1 represents rolling resistance dependence on velocity in addition to driveline losses and finally F_2 represents aerodynamic drag.

2.4. Energy consumption calculation

The engine fuel consumption is computed using equation (1). To monitor the battery SOC and thus help choose the appropriate driving mode, electric energy consumption is calculated at each instant. The battery is modelled as a voltage source with an internal resistance. The battery power (P_{batt}), current (I_{batt}), and SOC, are computed as follows:

$$P_{batt}(t) = P_{generator}(t) + P_{motor}(t) + P_{aux} \tag{16}$$

$$I_{batt}(t) = \frac{V_{OC}(SOC(t)) - \sqrt{V_{OC}^2(SOC(t)) - 4P_{batt}(t)R_{int}(SOC(t))}}{2R_{int}(SOC(t))} \tag{17}$$

$$P_{batt}(t) = I_{batt}(t)V_{batt}(t)(SOC(t)) \tag{18}$$

$$SOC(t) = \text{SOC}\,(t-1) - \frac{P_{batt}(t)}{C_{batt}} \tag{19}$$

The generator power $P_{generator}$ is a positive quantity as it charges the battery, the auxiliary power is a negative quantity as it discharges the battery and the electric motor power P_{motor} is negative during the traction mode and positive during the BER mode. The open-circuit voltage V_{OC} and the internal resistance R_{int} of the battery are considered from [13], where the nominal voltage is 201.6 V and the average internal resistance is 0.36 Ohms.

3. Energy management strategy

In this section, the different energy management strategies, controlling the vehicle model, will be investigated. The Optimal RB (Opt. RB) and optimized adaptive RB (Opt. A-RB) controllers are compared against a basic RB controller and the global optimal strategy of DP. The four EMS are detailed in the following section.

3.1. Basic RB control

The controller of the current vehicle is of RB type. it follows a charge depleting (CD) then a charge sustaining (CS) strategy [18]. The battery is depleted in the first part of the trip with the APU turned off, thus, completely utilizing the all-electric range of the PHEV. Once the battery SOC reaches its lower limit, namely 30%, the basic RB controller turns on the APU. The battery SOC is then maintained around 30% using a thermostat strategy for the entire remainder of the trip. A detailed explanation of how thermostat strategies function can be found in [19]. The engine runs at its optimal efficiency line in this case.

3.2. DP Control

Dynamic Programming is used as the global optimization routine. The WLTC drive cycle is used to emulate home-work commutes representing a recurrent trip and the results obtained will be analyzed in an approach like that used in [20] by the current co-author. Specific rules will be deduced from the DP control results and translated into an RB controller.

Since DP cannot be used with the graphical EMR model done on Simulink, an equivalent model was elaborated on MATLAB. The battery SOC was chosen to be the only state variable x(t), while the APU status (on/off) and the ICE speed were chosen as the two control variables, U1(t) and U2(t), respectively. Note that the engine is considered to operate on its optimal efficiency line so the engine torque is deduced from the engine speed. A value of 1 for U1(t) corresponds to APU On and a value of 0 corresponds to APU Off. The DP model use same equations as those introduced in the EMR model section 2.3. To make sure that the physical limits of the different components are respected in terms of speed, torque, power, and current, certain constraints were forced on the DP model.

Let $U_1 = \{u_o, ..., u_{n-1}\}$ & $U_2 = \{u_o, ..., u_{n-1}\}$ (where n is the time length of the route) be a certain APU status and speed strategy obtained from the DP model over the scheduled route, with initial and final SOCs being 80% and 30%, respectively. Then the goal is to find the optimal strategy U_{opt} that minimizes fuel consumption (the cost function C) over the scheduled route, formulated as

$$C = \int_0^n \dot{m}_{fuel}(x(t), u_1(t), u_2(t)) \tag{20}$$

The APU status u_1 (t) and engine speed u_2 (t) at any instant t are chosen with the future trip energy consumption taken into consideration. As a result, the optimal APU status and speed strategy is obtained with an optimal SOC trajectory x(t) for a scheduled route.

Since the optimal control strategy U_{opt} from DP cannot be implemented in real time, the Opt. RB controller will be constructed to replicate the optimal behavior as close as possible. The power

behavior of the drivetrain components is introduced in Figure 3 and plotted against the vehicle load power.

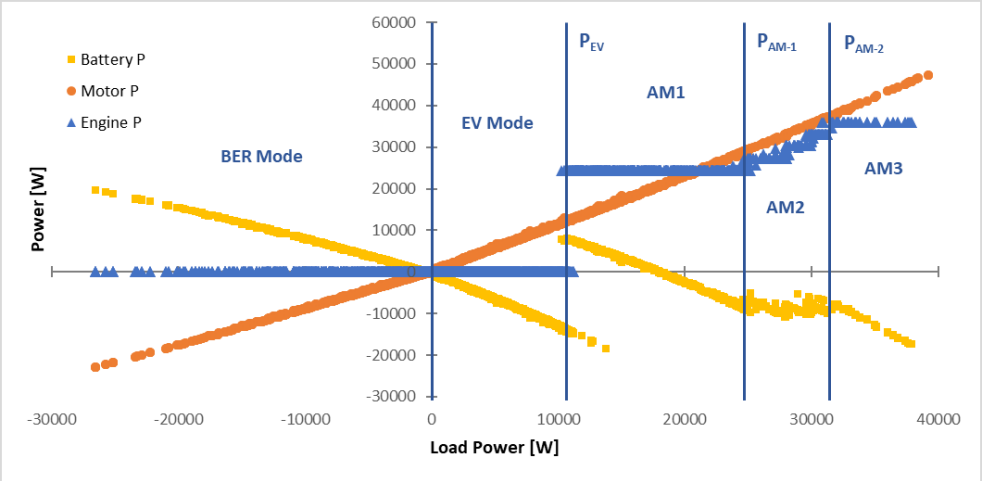

Figure 3: Power behavior of the drivetrain components under DP control for three repeated WLTPs

Five control modes are observed: break energy recovery (BER) mode, the electric vehicle mode, and three different APU modes.

1. In BER mode ($P_{load} < 0$), the APU is switched off and the EM is recovering kinetic energy and storing it in the battery.
2. In EV mode ($0 < P_{load} < P_{ev}$), the APU remains switched off while the EM withdraws all its power from the battery. As the load power exceeds the P_{ev} threshold, DP switches to APU mode. In Figure 3, the distance travelled is 70 km (three repeated WLTP drive cycles), and P_{ev} is 10.9 kW. This value was observed to change with the distance: the longer the route, the smaller P_{ev} is. Figure 4 shows the variation of P_{ev} as function of the distance (one to five repeated WLTPs). This decrease in the threshold suggests that for larger distances, the APU turns on more frequently, thereby preserving the battery energy until the end of the trip.
3. In APU mode ($P_{load} > P_{ev}$), three sub-modes are identified with a difference in engine operating speed. The first two sub-modes are separated by the threshold P_{apu-1} and the last two by P_{apu-2}. In APU mode 1, the APU delivers around 23 kW of electric power which is used to drive the motor, while the surplus power is stored in the battery. Once the load power surpasses P_{apu-1}, control switches to APU mode 2, where the APU power increases in a linear fashion as a function of the load power. In the last sub-mode (when $P_{load} > P_{apu-2}$), the APU delivers around 30 kW to drive the motor and the surplus is also stored in the battery. The thresholds P_{apu-1} and P_{apu-2} follow the same trend as P_{ev} and decrease with increasing trip distance battery.

3.3. Optimized RB Control

The optimized RB controller, according to the discussed modes above, can be written in a way to mimic the DP optimal behavior on the WLTP cycles. Based on Figure 4, the controller needs to obtain a new engine power-on threshold (P_{ev}) for each varying trip distance, in addition to the two APU thresholds P_{apu-1} and P_{apu-2}. DP can compute these parameters as soon as the drivers inputs their destination into the controller. The architecture of the Opt. RB controller is shown in Figure 5. It is like the one introduced in [20] by the present co-author, however, modified to fit this study's series PHEV.

The offline computation starts as soon as the driver inputs the desired destination. Using GPS and traffic management systems, the trip load simulator calculates the required P_{load}. DP receives the computed P_{load} and uses it to determine the optimal power thresholds for the selected route. The online computation aspect of the controller happens in real-time while the car is being driven. The driver power interpreter outputs the appropriate power demand to meet the vehicle load and satisfy driver commands. This demand is received by the power management controller which in turn outputs the correct APU command (whether to turn the engine on or off and at which speed) according to the thresholds resulted from DP. For the considered WLTP cycle, the driving conditions and commands of the Opt. RB control are summarized in Table 2.

The controller rules are derived from DP simulations based on the WLTP drive cycle, it is then important to mention that these rules are specific to the WLTP cycle and any difference in the scheduled route would lead to a diversion from the optimal DP results. Such differences in the scheduled route would translate into a lower or higher P_{load} on average and thus an early depletion or overcharge of the battery, respectively. Hence, DP would need to rerun the calculations and obtain updated thresholds and engine power levels for optimality.

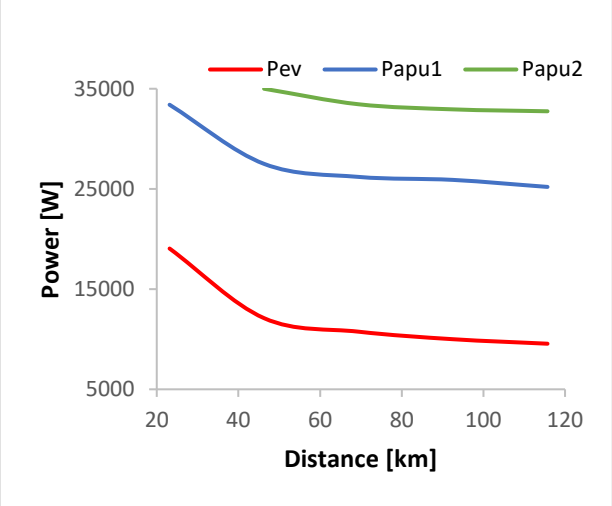

Figure 4: Thresholds variation function of the distance under optimal DP control

Table 2: Power management rules for the optimized rule-based controller

Driving Mode	Driving Condition	Driving Command Engine
Electric	$P_l < P_{ev}$	S_{Eng} = OFF P_{Eng} = 0
APU mode 1	$P_{ev} < P_l < P_{apu\text{-}1}$	S_{Eng} = ON P_{Eng} = 23 kW
APU mode 2	$P_{apu\text{-}1} < P_l < P_{apu\text{-}2}$	S_{Eng} = ON $P_{Eng} = 1.3*P_l + 7340$ kW
APU mode 3	$P_l > P_{apu\text{-}2}$	S_{Eng} = ON P_{Eng} = 33 kW
Regen-erative braking	$P_l < 0$	S_{Eng} = OFF P_{Eng} = 0

Where S_{Eng} is engine state (ON/OFF) and P_{Eng} is engine power.

3.4. Optimized Adaptive RB Control

To increase the functionality of the optimized RB controller, traffic intensity was taken into consideration. Since, as discussed in the introduction, this RB controller is being developed for repetitive home-work commutes, where the trip distance does not change, the traffic model considered was assumed to affect total trip time only and not the total distance. In this case, it is assumed that travelers will take no alternative routes to avoid traffic as the main concern is to study the impact of the vehicle average speed on the controller response and the corresponding energy consumption variation. Hence, the average velocity of the WLTP cycle would increase or decrease, respectively, with a decrease or increase in traffic intensity.

Four cases of increasing traffic were considered, compared to only one for decreasing traffic, since delays due to heavy traffic are more likely to happen in real life.

Table 3 summarizes the cases considered for the modified WLTP drive cycles with their respective total durations and average velocity ratios.

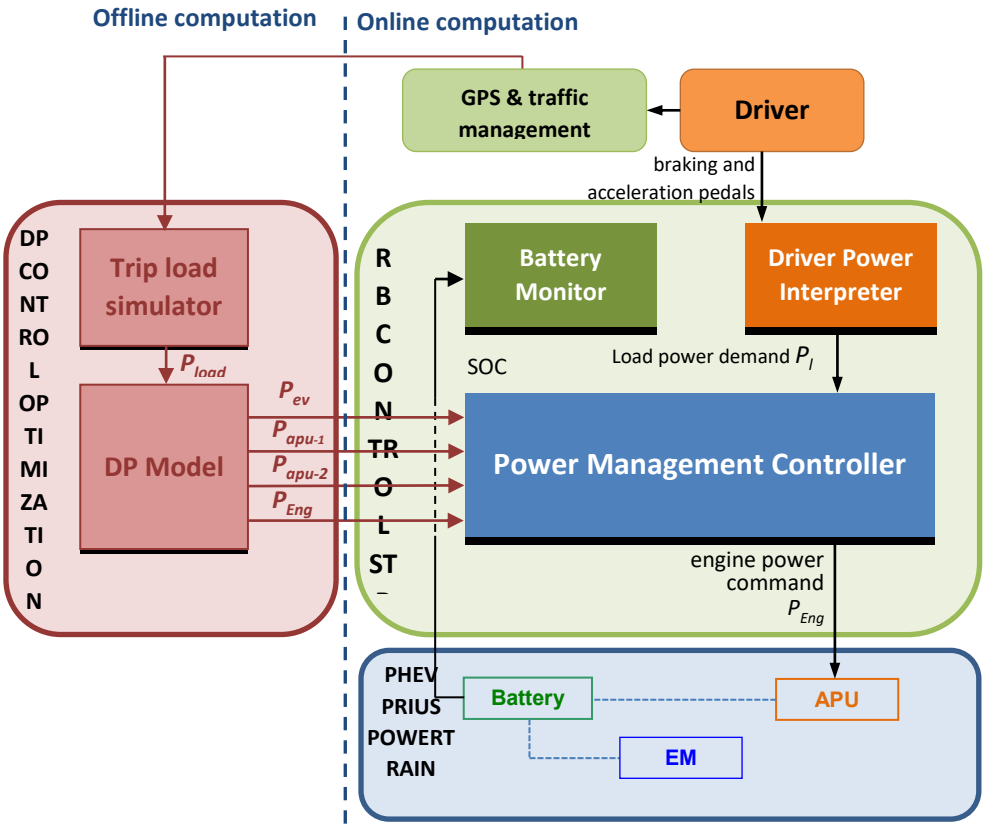

Figure 5: Optimized rule-based EMS architecture of Series PHEV

To simplify nomenclature, the original WLTP cycle is referenced as $WLTP_{baseline}$, while the modified WLTP cycles are referenced using the average velocity ratio, R_V, as follows:

$$R_V = \frac{V_{avg-modified}}{V_{avg-baseline}} \tag{21}$$

A similar procedure to that of section 3.2 is followed for the modified cycles to determine the new optimal power thresholds using DP. These updated thresholds were compared to the ones obtained for the $WLTP_{baseline}$ cycle, to establish a relationship between the two. For the case of the considered three and five repeated WLTP drive cycles, two general trends are observed:

1. For the case of $R_V > 1$ (decrease in traffic), the optimal power thresholds were higher than those of the $WLTP_{baseline}$.
2. For the case of $R_V < 1$ (increase in traffic), the optimal power thresholds were lower than those of the $WLTP_{baseline}$.

These results are in line with the following analysis: when the velocity of the drive cycle increases, the P_{load} requested also increases. Consequently, the new optimal power thresholds will be higher in order to avoid overcharging the battery as P_{load} is expected to surpass the baseline P_{ev} more frequently. Similarly, an increase in traffic intensity leading to a lower P_{load} results in lower optimal power thresholds.

It can then be concluded that the $WLTP_{baseline}$ power thresholds will need to be corrected by a certain factor, call it TCF_n (Traffic Correction Factor for Power Threshold n), to remain optimal, using the following equation:

$$P_{n-modified} = TCF_n * P_{n-baseline} \quad (22)$$

With n = ev, apu-1, or apu-2 depending on which threshold is being updated. Equation (28) can be reformulated and a traffic correction factor, TCF_n, is deduced:

$$TCF_n = \frac{P_{n-modified}}{P_{n-baseline}} \quad (23)$$

Figure 6 introduces the TCF for the thresholds TCF_{ev}, TCF_{apu-1}, and TCF_{apu-2}, as function of the varying average velocity ratio. The trends discussed above are highlighted in this figure where an $R_V > 1$ would output a TCF > 1, and thus, leading to higher thresholds. Similar logic is applied when $R_V < 1$. It is interesting to note that for an $R_V = 1$ (signifying $WLTP_{baseline}$) the TCFs all intersect at the value 1, meaning no correction is done to the baseline thresholds.

Table 3: The different WLTP velocity modifications

Rv	Duration [s]	V_{avg} [km/h]	case
1.1	4912	50.8	Traffic Decrease
1	5403	46.2	Baseline
0.9	6004	41.6	Traffic Increase
0.8	6754	37	Traffic Increase
0.7	7719	32.4	Traffic Increase
0.6	9006	27.7	Traffic Increase

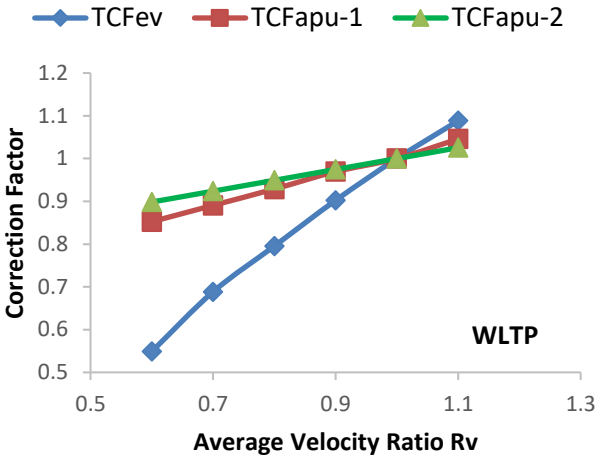

Figure 6: Traffic correction factor as function of average velocity ratio Rv

From the above analysis, the Opt. RB EMS architecture is modified to include a Traffic Monitoring Module that receives the updated average velocity from the Traffic Management System and the thresholds P_{ev}, P_{apu-1}, and P_{apu-2} from DP. Using equation (29) and the correlations shown in Figure 6, the Traffic Monitoring Module outputs the updated optimal thresholds to the Power Management Controller.

4. Results

4.1. Optimized RB Controller

Figure 7 shows a comparison of the engine fuel consumption under the basic RB controller, the Opt. RB controller and the DP controller. Opt. RB control shows 1% to 2% increase in fuel consumption relative to the DP controller over distances covering up to 118 km (one to five repeated WLTP cycles) and 13% to 16% decrease in FC relative to the basic RB controller. This signifies that a remarkable reduction in computational requirements from DP optimal control to Opt. RB control does not necessarily lead to deteriorated fuel economy.

Figure 8 and Figure 9 are from simulations run on three repeated WLTP cycles and used as an example of the obtained results. From the battery SOC in Figure 8, we can notice that the Opt. RB controller charges the battery slightly higher than DP and this is due to the minor approximations considered upon deriving the power thresholds, mainly data filtering and fittings. The basic RB

controller follows the charge depleting then charge sustaining strategy previously mentioned, which explains why the fuel consumption is way higher than the optimal consumption. Obviously, DP cannot be perfectly emulated by a set of rules and these slight differences can be noticed in Figure 9 where the engine speed of the Opt. RB controller diverges from the optimal strategy at some points. These load power points lie near the thresholds (P_{ev}, P_{apu-1}, P_{apu-2}) used in the driving commands, and as some approximations and data filtering are considered upon deriving the power thresholds, it will result in a different driving mode than that chosen by DP.

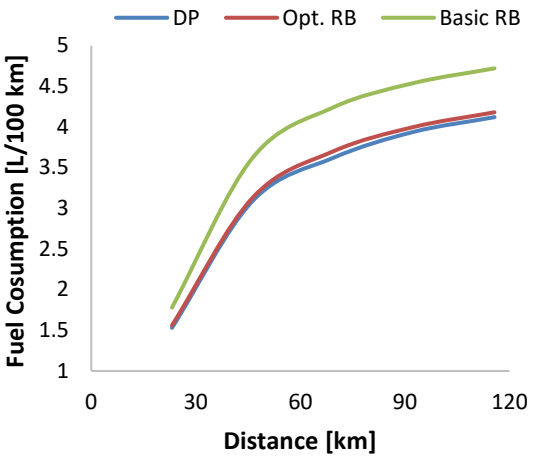

Figure 7: Fuel consumption comparison between DP, basic RB, and Opt. RB control

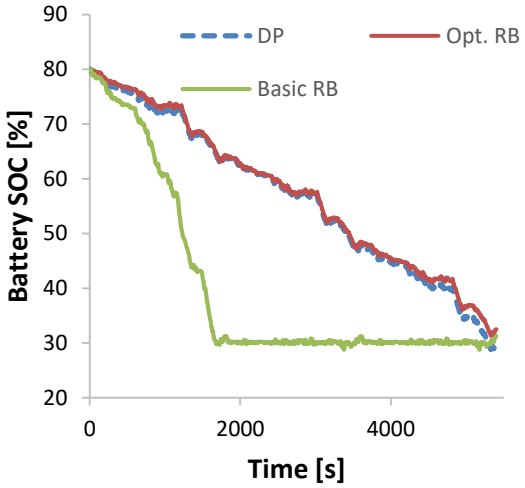

Figure 8: Battery SOC comparison between DP, basic RB, and ORB control over three repeated WLTPs.

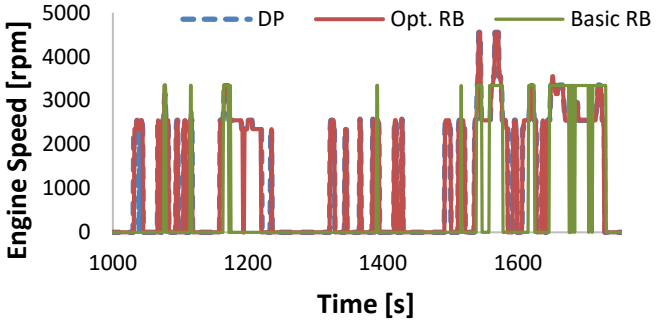

Figure 9: Engine speed comparison between DP, basic RB, and ORB control over part of three repeated WLTPs

4.2. Optimized Adaptive RB Controller

The engine fuel consumption comparison results under the DP, Opt. RB and Opt. A-RB controllers, over three and five repeated WLTP cycles are presented in Figure 10.

Figure 10 shows that if the thresholds of the $WLTP_{baseline}$ cycle (Opt. RB) are used for the modified cycles, deviations in optimal FC results range from 6% for an $R_V$of 0.9 to 22% for an $R_V$of 0.6. However, using the Opt. A-RB controller, deviations from optimal FC results range from 2% for an $R_V$of 0.9 to a maximum of 5% for an $R_V$of 0.6. These results highlight the need for an Opt. A-RB controller in case of traffic changes in the scheduled route to keep FC results close to optimal. Such an optimization would prove extremely useful for everyday commutes where a small improvement in fuel economy would lead to large long-term fuel savings.

These results were confirmed by repeating the same procedure for five repeated WLTPs, which yielded equivalent results. The battery SOC variation, for three repeated WLTPs, at an Rv of 0.9 is shown in Figure 11, which highlights how the Opt. RB controller leads to an early depletion of the battery energy and then switches to the basic RB control for the rest of the trip. This in turn explains the higher FC results compared to the Opt. A-RB shown in Figure 10.

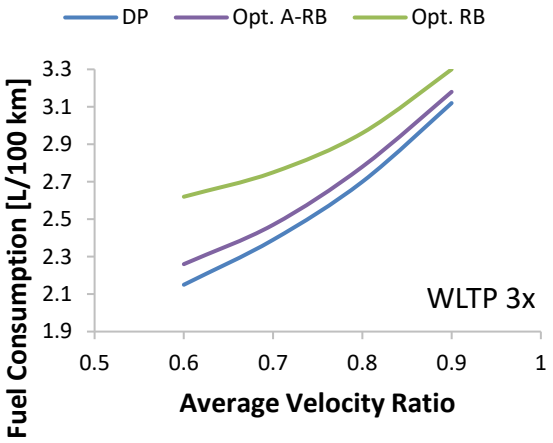

Figure 10: Fuel consumption comparison between DP, Opt. RB, and Opt. A-RB control over three repeated WLTP cycles.

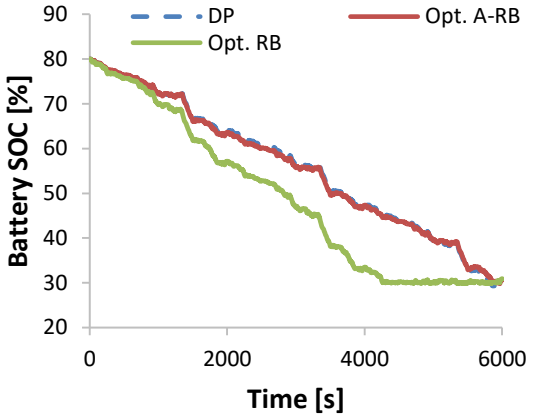

Figure 11: Battery SOC comparison between DP, Opt. RB, and Opt. A-RB over three repeated WLTPs with Rv =0.9

5. Conclusion

This paper presents a systematic methodology to powertrain modeling practitioners to develop an optimized RB controller based on the global optimization technique DP. The study incorporates a series PHEV and the main application of this study is recurrent trips that may represent home – work commutes. The optimal control strategy chosen by DP over repeated WLTP drive cycles is analyzed and emulated by a set of rules used by the RB controller. blended CS/CD mode of the battery energy was observed to be optimal in terms of fuel savings conserving the electric energy until the end of the trip. The proposed controller is further adapted to consider variation in trip distance and traffic intensity along the road. The proposed Opt. A-RB controller shows a promising powertrain components behavior and fuel consumption compared to DP. It is important to note that optimization was done based on repeated WLTP drive cycles and as such the results are only applicable to that specific repeating route profile. However, same methodology can be used to optimize the energy management strategy for any drive cycle.

References

[1] Panday A, Bansal HO. A review of optimal energy management strategies for hybrid electric vehicle. Int J Veh Technol 2014;2014. doi:10.1155/2014/160510.

[2] Salmasi FR. Control Strategies for Hybrid Electric Vehicles: Evolution, Classification, Comparison, and Future Trends. Veh Technol IEEE Trans 2007;56:2393–404. doi:10.1109/TVT.2007.899933.

[3] Enang W, Bannister C. Modelling and control of hybrid electric vehicles (A comprehensive review). Renew Sustain Energy Rev 2017;74:1210–39. doi:10.1016/j.rser.2017.01.075.

[4] Zhang P, Yan F, Du C. A comprehensive analysis of energy management strategies for

hybrid electric vehicles based on bibliometrics. Renew Sustain Energy Rev 2015;48:88–104. doi:10.1016/j.rser.2015.03.093.

[5] Tate ED, Boyd SP. Finding Ultimate Limits of Performance for Hybrid Electric Vehicles, 2000. doi:10.4271/2000-01-3099.

[6] Sundström O, Guzzella L, Soltic P. Optimal Hybridization in Two Parallel Hybrid Electric Vehicles using Dynamic Programming. IFAC Proc Vol 2008;41:4642–7. doi:10.3182/20080706-5-KR-1001.00781.

[7] Grizzle JW. Power management strategy for a parallel hybrid electric truck. IEEE Trans Control Syst Technol 2003;11:839–49. doi:10.1109/TCST.2003.815606.

[8] Song P, Guan E, Zhao L, Liu S. Hybrid Electric Vehicles with Multilevel Cascaded Converter using Genetic Algorithm. 2006 1ST IEEE Conf Ind Electron Appl 2006:1–6. doi:10.1109/ICIEA.2006.257211.

[9] Zhang B, Chen Z. Multi-objective parameter optimization of a series hybrid electric vehicle using evolutionary algorithms. Veh Power … 2009:921–5. doi:10.1109/VPPC.2009.5289749.

[10] Kim N, Lee D, Cha SW, Peng H. Optimal Control of a Plug-In Hybrid Electric Vehicle (PHEV) Based on Driving Patterns. Evs24 2009 2009:1–9.

[11] Stockar S, Marano V, Rizzoni G, Guzzella L. Optimal Control for Plug-in Hybrid Electric Vehicle Applications. Am Control Conf 2010:5024–30. doi:10.1109/ACC.2010.5530752.

[12] Pisu P, Rizzoni G. A supervisory control strategy for series hybrid electric vehicles with two energy storage systems. 2005 IEEE Veh Power Propuls Conf 2005:8 pp. doi:10.1109/VPPC.2005.1554534.

[13] Onori S, Serrao L, Rizzoni G. Adaptive Equivalent Consumption Minimization Strategy for Hybrid Electric Vehicles. Proc ASME Dyn Syst Control Conf 2010;2010:499–505. doi:10.1115/DSCC2010-4211.

[14] Wirasingha SG, Emadi A, Sÿ NO. Classification and Review of Control Strategies for Plug-in Hybrid Electric Vehicles. Strategy 2009;60:907–14.

[15] Mohammadian M, Bathaee MT. Motion control for hybrid electric vehicle. Conf Proc IPEMC 2004 4th Int Power Electron Motion Control Conf (IEEE Cat No04EX677) 2004:1490–4.

[16] EMRwebsite - Home n.d. http://www.emrwebsite.org/ (accessed February 27, 2018).

[17] Liu W. Introduction to hybrid vehicle system modeling and control. John Wiley & Sons; 2013.

[18] Shiau CSN, Samaras C, Hauffe R, Michalek JJ. Impact of battery weight and charging patterns on the economic and environmental benefits of plug-in hybrid vehicles. Energy Policy 2009;37:2653–63. doi:10.1016/j.enpol.2009.02.040.

[19] Kim M, Jung D, Min K. Hybrid thermostat strategy for enhancing fuel economy of series hybrid intracity bus. IEEE Trans Veh Technol 2014;63:3569–79. doi:10.1109/TVT.2013.2290700.

[20] Mansour CJ. Trip-based optimization methodology for a rule-based energy management strategy using a global optimization routine: The case of the Prius plug-in hybrid electric vehicle. Proc Inst Mech Eng Part D J Automob Eng 2016;230:1529–45. doi:10.1177/0954407015616272.